Experiments on the flow past a circular cylinder at low Reynolds numbers

By D. J. TRITTON
Cavendish Laboratory, Cambridge

(Received 25 February 1959)

Part I describes measurements of the drag on circular cylinders, made by observing the bending of quartz fibres, in a stream with the Reynolds number range 0·5–100. Comparisons are made with other experimental values (which cover only the upper part of this range) and with the various theoretical calculations.

Part II advances experimental evidence for there being a transition in the mode of the vortex street in the wake of a cylinder at a Reynolds number around 90. Investigations of the nature of this transition and the differences between the flows on either side of it are described. The interpretation that the change is between a vortex street originating in the wake and one originating in the immediate vicinity of the cylinder is suggested.

Introduction

This paper is concerned with two-dimensional flow past a circular cylinder. The Reynolds number, R, is defined throughout on the diameter of the cylinder and the velocity, U, far from it. Directions are referred to in terms of the Cartesian co-ordinates, x, y and z, which are respectively in the direction of flow far from the cylinder, perpendicular to both this and the cylinder, and parallel to the cylinder.

It is well known that as R is increased from low values for which approximate solutions of the Navier–Stokes equations can be found, a complex sequence of events takes place. At a Reynolds number estimated at 3·2 by Nisi & Porter (1923), 5 by Taneda (1956), and 6 by Homann (1936), the flow separates from the cylinder before reaching the rear generator and a pair of attached eddies forms behind the cylinder.

The Reynolds number of the first appearance of a vortex street behind the cylinder is also rather variably estimated. It is common to take it as 40, though Taneda (1956), puts it as low as 30. It is often supposed (e.g. Goldstein 1938, § 183) that the street is produced by the attached eddies stretching farther and farther downstream, becoming distorted, and then being shed alternately from the sides of the cylinder. However, an inspection of the flow (as photographed for instance by Homann (1936)) suggests that at Reynolds numbers only a little above 40 the street develops out of an instability in the wake. The wind-tunnel experiments of Kovasznay (1949) lend support to this view. Further the work of Hollingdale (1940) and Taneda (1958) on the wake of a flat plate at zero

incidence has shown conclusively that a vortex street can develop independently of attached eddies.

According to Roshko (1954), the mode of flow first appearing at $R \sim 40$ continues until $R \sim 150$ when the motion of the vortices becomes less regular and turbulence is produced downstream.

Part I of this paper describes experiments that give values for the drag on a cylinder in the range $0{\cdot}5 < R < 100$—a range of some interest in view of the sequence of changes that occurs within it. Part II gives experimental evidence for there being a further change at $R \sim 90$, and suggests a qualitative explanation of this.

Part I. The Drag on Circular Cylinders for $0{\cdot}5 < R < 100$

The approximate solutions of the Navier–Stokes equations give theoretical values for the drag coefficient when the Reynolds number is rather less than 1. The previous lowest R at which an experimental value was obtained was 4·22 and good agreement between different experimental investigations did not begin until about $R = 20$. It has been, however, common practice to interpolate values in the intermediate range. The range is too long for this to be accurate and the interpolation would seem particularly subject to error in view of the fact that the first appearance of attached eddies occurs within it. Hence, when I was doing some experiments that provided some information on the drag coefficient in this low R region, it seemed worthwhile extending them to fill in this gap in the R–C_D curve.

The experiments concerned were a series of calibrations of quartz-fibre anemometers for measuring the low air speeds of free convective flows. This instrument was developed by Schmidt (1934) (see also, Schmidt & Beckmann (1930)), but has not previously been used as an absolute measure. An advantage of so using it is that it enables the measurements to be extended to speeds lower than those available for calibration.

In the author's arrangement of the instrument the quartz-fibre is cemented into the end of a piece of hypodermic tubing. The free end of the fibre is viewed through a tele-microscope with an eyepiece scale previously calibrated against a stage graticule. The objective has a working distance of about 4 cm, which is large enough for the tele-microscope not to affect the flow round the fibre.

If simple bending moment theory is supposed to apply, the deflexion of the end of the fibre produced by a force F per unit length normal to its axis is

$$h = \frac{8Fl^4}{\pi E d^4},$$

where l, d, and E are the length, diameter and Young's modulus of the fibre. If F is taken as the drag produced by a stream of air with velocity U flowing past an infinite circular cylinder, then the drag coefficient, defined as

$$C_D = \frac{F}{\frac{1}{2}\rho U^2 d}$$

(ρ is the density of air), is given by

$$C_D = \frac{\pi E d^3 h}{4\rho U^2 l^4}.$$

There are a number of requirements on the quantities involved for this result to be useful. (i) Simple bending moment theory must apply. It was calculated that, for errors to be less than 1 %, this requires $l/h > 15$. (ii) The cylinder must be long enough for it to be regarded as effectively infinite. The smallest value of l/d for the author's fibres was 150; judging by the results of Wieselsberger (1922) for finite cylinders this is perhaps not really large enough, but the results obtained with this fibre could be fitted in with those from fibres of much larger l/d. (iii) h must be an order of magnitude larger than d or it is not accurately measurable.

All these conditions could be satisfied with a set of fibres with diameters in the range 20–100 μ and lengths in the range 1–3 cm, which then fulfils the dual purpose of determining C_D in the range $0{\cdot}5 < R < 100$ (some overlap with the already established range was thought desirable as a check on the accuracy of the technique) and measuring air velocities down to 10 cm/sec.

Of the quantities that are needed for calculating R and C_D from observed values of U and h, the fibre diameter is the most difficult to measure and this is the limiting factor on the accuracy of the experiments. The diameters of the larger fibres were measured with a travelling microscope. For the smaller ones this was not sufficiently accurate and a wedge fringe optical interference method with reflected sodium light was used instead. It was also found necessary to measure the Young's modulus for each fibre diameter. This was done by determining the resonant frequencies of a mounted fibre. This work has already been described elsewhere (Tritton 1959) as it indicated that the modulus varies with diameter. In terms on the nth resonant frequency, ν_n, the Young's modulus is

$$E = \frac{64\pi^2 l^4 \rho_Q}{d^2}\left(\frac{\nu_n}{\phi_n^2}\right)^2,$$

where ρ_Q is the density of fused quartz and ϕ_n is the nth root of

$$\cos\phi \cosh\phi = -1$$

(Tritton 1959). Hence,

$$C_D = \frac{16\pi^3 d \rho_Q h}{\rho U^2}\left(\frac{\nu_n}{\phi_n^2}\right)^2.$$

The diameter dependence is thus reduced from third order to first, giving a fortunate increase in accuracy.

The resonance measurements also indicated rather better than the diameter measurements when the fibre was not truly circular; in this case each resonance became a doublet. Departures from circular cross-sections (calculated assuming elliptical ones) were in the worst cases around 3 % and usually rather less than this.

The measurements of the deflexions produced by the air flow were carried out in one of the Cavendish Laboratory's wind-tunnels. This is fitted with a manometer that measures speeds down to 250 cm $\sec^{-1}$. The tunnel will, however, run

Fibre and method of velocity measurement	Pressure and temperature	Velocity, U (cm sec^{-1})	Deflexion, h (cm)	Reynolds no., R (Absolute measurements)	Drag coefficient C_D (Absolute measurements)
Fibre 1					
$l = 1{\cdot}70$ cm; $d = 0{\cdot}00194$ cm;	765 mm Hg,	31·9	0·0413	0·416	18·6
$\nu_n/\phi_n^2 = 16{\cdot}2$ sec^{-1}.	20·8° C	38·2	0·0501	0·494	15·8
Eddy frequency with $50 < R < 150$		39·7	0·0556	0·518	16·2
		41·15	0·0577	0·532	15·7
		44·5	0·0643	0·576	15·0
		48·7	0·0721	0·634	14·0
		50·7	0·0765	0·661	13·7
		56·85	0·0883	0·741	12·6
		60·5	0·0961	0·783	12·1
		63·4	0·1036	0·820	11·9
		64·95	0·1063	0·845	11·6
	752 mm Hg, 20·3° C	30·2	0·0375	0·387	19·2
Fibre 2					
$l = 1{\cdot}27$ cm; $d = 0{\cdot}00197$ cm;	760 mm Hg,	49·2	0·0226	0·650	14·8
$\nu_n/\phi_n^2 = 29{\cdot}45$ sec^{-1}.	19·1° C	54·3	0·0254	0·719	13·6
Combination of heat-pulse tracing		73·3	0·0356	0·968	10·5
and eddy frequency with		87·8	0·0460	1·16	9·49
$50 < R < 150$		97·2	0·0530	1·29	8·85
		99·5	0·0544	1·32	8·69
		112·7	0·0646	1·50	8·05
		129·6	0·0788	1·72	7·41
Fibre 3					
$l = 3{\cdot}12$ cm; $d = 0{\cdot}00442$ cm;	744 mm Hg,	36·7	0·0362	1·06	11·7
$\nu_n/\phi_n^2 = 10{\cdot}07$ sec^{-1}.	20·6° C	44·4	0·0462	1·28	10·2
Combination of heat-pulse tracing		50·4	0·0554	1·45	9·07
and eddy frequency with		58·3	0·0668	1·68	8·13
$50 < R < 150$	769 mm Hg,	55·8	0·0626	1·64	8·19
	22·2° C	57·8	0·0666	1·70	8·13
		69·35	0·0858	2·04	7·26
		76·4	0·0982	2·25	6·86
		81·35	*0·1070*	*2·40*	*6·56*
		91·2	0·1248	2·69	6·11
		103·6	0·1485	3·05	5·64
		109·8	0·1628	3·24	5·50
		119·2	0·1817	3·51	5·20
Fibre 6*					
$l = 2{\cdot}07$ cm; $d = 0{\cdot}00753$ cm;	768 mm Hg,	297	0·0224	15·3	2·20
$\nu_n/\phi_n^2 = 36{\cdot}4$ sec^{-1}.	16·5° C	335	0·0292	17·3	2·25
Manometer (calibrated by heat-		429	0·0466	22·1	2·20
pulse tracing and by Pitot tube		454	0·0446	23·4	1·87
+ Chattock manometer)		530	0·0596	27·4	1·83
		553	0·0686	28·5	1·94
		586	0·0732	30·2	1·85
		660	0·0896	34·0	1·78
		738	0·1068	38·1	1·69
		808	0·1218	41·7	1·62

* Fibre 6 showed slight hysteresis, giving rather more scatter than other fibres.

TABLE 1

Fibre and method of velocity measurement	Pressure and temperature	Velocity, U (cm sec^{-1})	Deflexion, h (cm)	Reynolds no., R	Drag coefficient C_D
				Absolute measurements	
Fibre 7					
$l = 1{\cdot}12$ cm; $d = 0{\cdot}00745$ cm;	769 mm Hg,	620	0·0062	31·4	1·58
$E = 5{\cdot}95 \times 10^{11}$ dyne cm^{-2}.	18·0° C	759	0·0086	38·5	1·46
Manometer		918	0·0134	46·6	1·56
		967	0·0138	49·0	1·45
		1042	0·0162	52·8	1·46
		1194	0·0214	60·5	1·47
		1221	0·0214	61·9	1·41
		1275	0·0244	64·6	1·47
Fibre 8					
$l = 2{\cdot}11$ cm; $d = 0{\cdot}01125$ cm;	771 mm Hg,	587	0·0188	44·9	1·46
$E = 5{\cdot}95 \times 10^{11}$ dyne cm^{-2}	18·2° C	597	0·0184	45·7	1·38
Manometer		730	0·0276	55·8	1·39
		836	0·0350	64·0	1·34
		844	0·0358	64·6	1·34
		900	0·0398	68·9	1·31
		990	0·0464	75·8	1·27
		1016	0·0510	77·8	1·32
		1082	0·0554	82·8	1·26
		1182	0·0660	90·5	1·26
		1237	0·0712	94·7	1·24
		1272	0·0764	97·3	1·26
		1377	0·0878	105	1·24
		1442	0·0962	110	1·24
		1508	0·1052	115	1·24
				'Fitted' values	
Fibre 4					
$l = 2{\cdot}28$ cm; $d \sim 0{\cdot}0047$ cm.	751 mm Hg,	77·8	0·0228	2·44	6·47
Eddy frequency with $50 < R < 150$	16·8° C	91·0	0·0276	2·86	5·77
		121·5	0·0418	3·82	4·91
		155	0·0580	4·86	4·20
		174	0·0706	5·51	3·99
		208	0·0900	6·52	3·62
		237	0·1088	7·45	3·37
		257	0·1270	8·09	3·33
	747 mm Hg,	49·2	0·0130	1·54	9·38
	16·9° C	67·0	0·0190	2·09	7·40
		75·3	0·0216	2·36	6·67
		116	0·0390	3·61	5·08
Fibre 5					
$l = 1{\cdot}33$ cm; $d \sim 0{\cdot}0043$ cm.	749 mm Hg,	165	0·0102	4·81	4·45
Eddy frequency with $R > 300$	16·9° C	243	0·0180	7·10	3·61
(formula given by Roshko (1954))		324	0·0270	9·44	3·06
		342	0·0298	9·95	3·07
		391	0·0344	11·4	2·67
		449	0·0422	13·1	2·51
		539	0·0566	15·7	2·30
		646	0·0734	18·8	2·09
		756	0·0922	22·0	1·91

TABLE 1 (*cont.*)

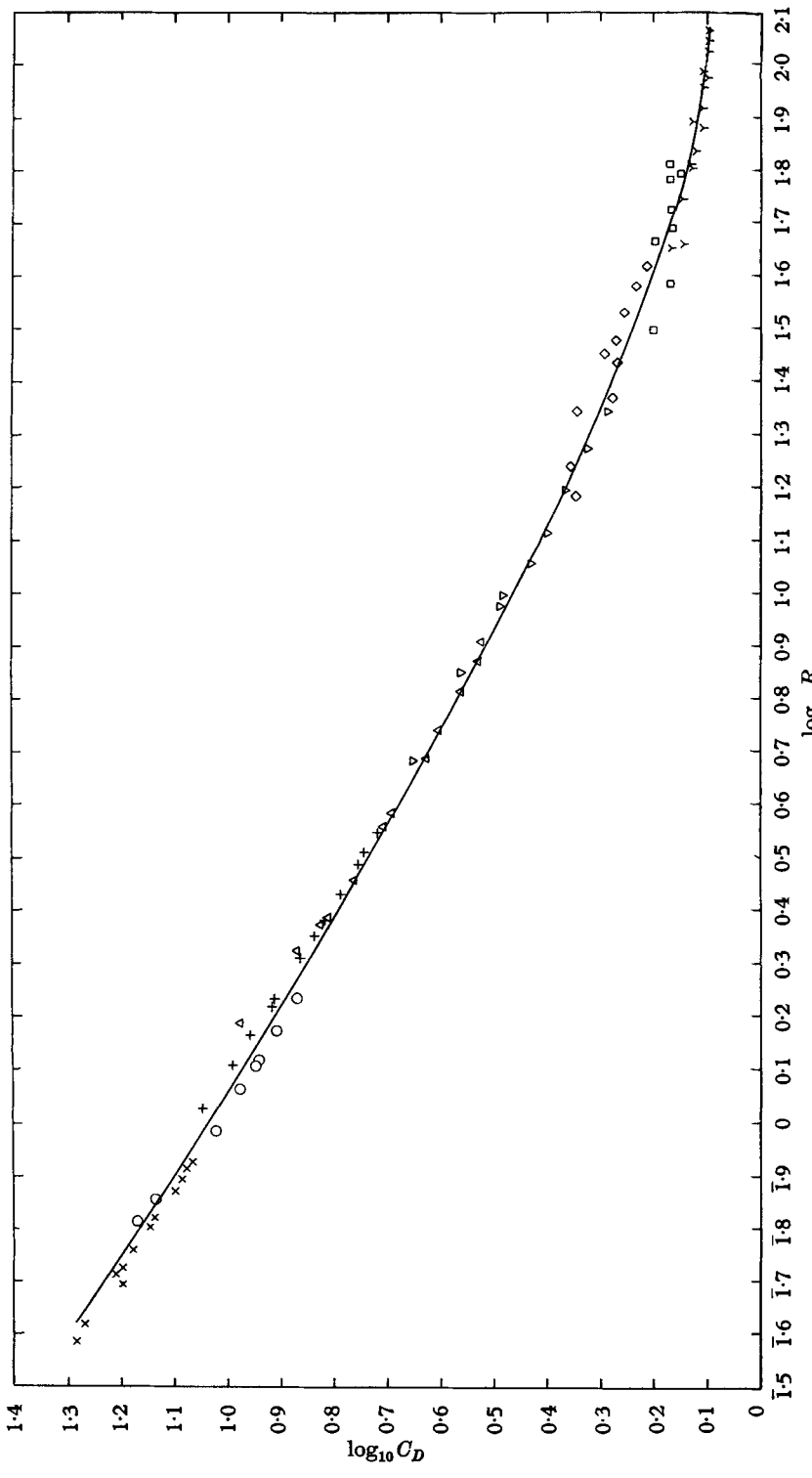

FIGURE 1. Plot of $\log C_D$ against $\log R$ showing all the observations listed in table 1. The line is an estimated mean curve, bearing in mind that the slope of the line for each fibre is known with greater accuracy than its position. This line is used for comparison purposes in figures 2 and 3. Absolute measurements: ×, fibre 1; ○, fibre 2; +, fibre 3; ◇, fibre 6; □, fibre 7; Y, fibre 8. 'Fitted' points: △, fibre 4; ▽, fibre 5.

as slowly as 30 cm sec^{-1}, so that other methods had to be developed for the lower speed runs. That first adopted was the measurement of the frequency of vortices in the street behind a second (thicker) cylinder (Roshko 1954). It was during this work that the frequency discontinuity that is to be described in Part II was discovered and the experimental methods will be recounted in more detail there. As a result of the existence of this discontinuity the formula given by Roshko for the velocity producing an observed frequency is less reliable than previously thought. Hence, some of the quartz fibres were also calibrated by tracing heat pulses down the wind-tunnel. The pulses were produced by a 50 c/s alternating current (giving 100 c/s temperature variations) in a 25 μ diameter wire stretched across the tunnel. The voltage supply to this was put across the X-plates of an oscilloscope, on the Y-plates of which was the amplified output of a hot-wire detector in the heat-wake. The velocity could then be measured by observing the variations in the resulting Lissajous figure as the detector was moved down the tunnel. At very low speeds the temperature variations are destroyed by diffusion too quickly for this technique to work. It was, therefore, necessary to use the eddy frequency method incorporating a correction, obtained from the results of the other runs, for the deviations from Roshko's result. This 'mixing' of velocity measuring method undoubtedly resulted in a small loss of accuracy.

The results are presented in table 1 and plotted on a log-log scale in figure 1. For two of the fibres the points are termed 'fitted'; this means that full measurements of the fibre diameter and Young's modulus were not made, but the results were adjusted to fit in with those of other fibres. Fibres were sometimes broken during the diameter measurements which could then not be completed. Since the U *vs* h measurements give the slope of the $\log R$ *vs* $\log C_D$ curve, independently of the constants of the fibre, the adjustment consisted of moving all the points for one fibre without changing their relative position.

The overall accuracy of the figures given for the drag coefficient is estimated at around 6 %. The internal accuracy of the points for a single fibre is, however, much better and is estimated at around 2 %.

Figure 2 compares the results for the drag coefficient with those of Relf (1913) and of Wieselsberger (1921).* (The former made direct measurements of the force on a frame of wires; the latter observed the deflexion of a weight suspended on a wire in the air-stream.) The agreement is good at the centre of the range of overlap. Probably the lowest R points of the other workers were stretching their techniques a little beyond their limits. The disagreement of about 10 % around $R = 100$ is more puzzling. Four comments may be made about my results in this region of R:

(i) The length–diameter ratio tends to be lower for the fibres used at the higher Reynolds numbers, which might slightly accentuate the decrease in C_D.

(ii) A similar effect might arise for the points of each individual fibre, from the fact that at the higher speeds it is more bent and so less exactly perpendicular to the flow.

* Though Wieselsberger describes his experiments in this paper, his actual figures are given in Prandtl (1923).

(iii) There was a rather large scatter in the diameter measurements of fibre 8 which was probably due to variations along its length (of maybe 2 %).

(iv) It is possible that there was some interaction between fibre 8 and the vortex street behind it. The street frequency was typically around the fifth fibre resonance, which is a sufficiently high order for it not to be easily stimulated. However, the possession of resonant frequencies by the fibre could lead to a modification of the street frequency and so of the drag. For *a few* of the points the fibre was vibrating slightly (though this is thought to be due to resonance of the wind-tunnel motor), but there is good agreement between these and points for which the fibre appeared quite stationary.

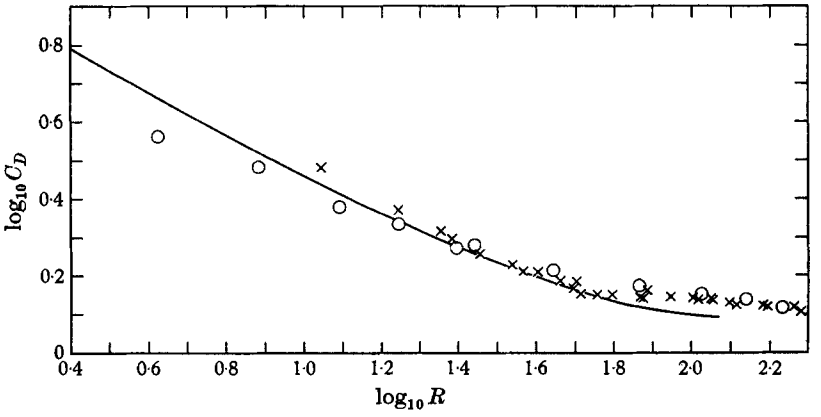

FIGURE 2. Comparison with other experimental measurements of the drag coefficient. ×, Relf; ○, Wieselsberger; —, Tritton.

Points such as these were taken into account in the above estimate of 6 % accuracy, but they do perhaps suggest that the error may be rather larger at the high R end of the curve. It seems unlikely, however, that this is sufficient to fully explain the difference from Relf and Wieselsberger, and I think that, despite their good mutual agreement, their measurements must be on the high side. Since neither author gives any discussion of systematic errors, it is difficult to tell how likely this is.

Figure 3 compares the present experimental results with the various theoretical calculations:

(i) The low Reynolds number solution of the Oseen equation, due to Lamb (1911).

(ii) Both Bairstow, Cave & Lang (1923) and Tomotika & Aoi (1950) have extended the solution of the Oseen equation to higher Reynolds number. Their results for the drag coefficient are in close agreement and are given as a single line in figure 3. This approach to the problem has been criticized by Proudman & Pearson (1957) on the grounds that the approximation involved in Lamb's solution is no worse than that already involved in the Oseen equation.

(iii) Southwell & Squire (1934) give a solution for Reynolds number 2, by a method similar to Oseen's, but supposing the convection to be conditioned by the irrotational velocities instead of the undisturbed velocity.

(iv) Kaplun (1957) gives a solution obtained by matching an Oseen solution far from the cylinder with a Stokes solution close to it. The effect is to give a third term in the low Reynolds number expansion, of which Lamb's solution gives the first two.

(v) Relaxational solutions of the Navier–Stokes equations: at $R = 1$ and 10 due to Allen & Southwell (1955); a rough solution at $R = 10$ (Thom 1929) and a detailed one at $R = 20$ (Thom 1933); and at $R = 40$ by Kawaguti (1953) and Apelt (1959), independently.

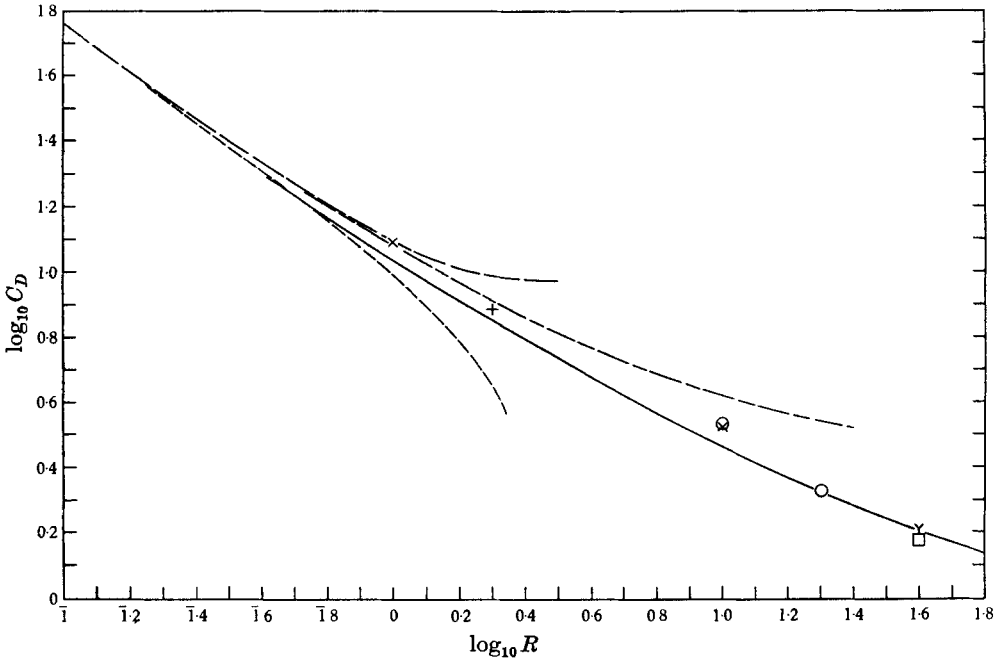

FIGURE 3. Comparison of the experimental curve with the various theoretical evaluations of the drag coefficient. —, Experimental (Tritton); — — —, Lamb; – · –, Bairstow, Cave & Lang; also Tomotika & Aoi; - - - -, Kaplun; +, Southwell & Squire; ×, Allen & Southwell; ○, Thom; Y, Kawaguti; □, Apelt.

The experimental points fit in satisfactorily with the overall picture given by these various theories. There is good agreement with the relaxation calculations particularly with Thom's at $R = 20$ and Kawaguti's at $R = 40$, which are thought to be particularly reliable calculations. At low Reynolds numbers, the experimental curve does not join on quite smoothly to the common curve of the theories, but the disagreement is within the limits of experimental error and there can be little doubt that the two curves should coincide for R less than about 0·6. The agreement with Kaplun's solution at rather higher Reynolds numbers than the others is satisfactory since this is a higher-order approximation.

The Reynolds number range covered by the present measurements includes the first appearance both of attached eddies and of the vortex street; the results should thus show what effects these changes have on the drag coefficient. Since the relative accuracy of points obtained from the same fibre is greater than

those from different fibres, the individual U *vs* h curves of the various fibres have been inspected. These show that there is no sharp discontinuity in the drag in either of the ranges $3 < R < 6$ and $30 < R < 45$. There is, however, some indication of a discontinuity around $R = 80$; this is presumably related to the phenomenon described in Part II and will be discussed there.

Part II. A Transition in Flow Past a Cylinder at $R \sim 90$

1. The discontinuity in frequency and amplitude

Roshko (1954) gives the relationship between the Reynolds number and the Strouhal number S (non-dimensional eddy frequency) as

$$S = \frac{nd}{U} = 0{\cdot}212 - \frac{4{\cdot}5}{R}$$

in the range $50 < R < 150$. (Here n is the frequency in the vortex street as given by a detector fixed relative to the cylinder.) In this range the street just dies out slowly as it is traced downstream; there is no turbulence.

Whilst I was using this result for measuring velocities (as described in Part I), it became apparent that it is not quite correct; there is a small discontinuity in the velocity-frequency curve. This is shown in figure 4, where frequency is plotted against velocity for three runs. The frequency was measured by putting the amplified output of a hot-wire anemometer placed in the wake onto the Y-plates of an oscilloscope and adjusting the frequency of an electronic oscillator on X-plates until a Lissajous figure was obtained. The velocity was obtained by recalibrating the quartz-fibre as described in Part I.

In each diagram of figure 4 the points fall on two separate lines; the transition between the two involves a sudden decrease of around 5 % in frequency as the velocity is increased. The broken line on each plot is the velocity-frequency dependence given by Roshko's formula. This does not come in just the same position relative to the points each time. The reason is that the internal accuracy of a single run is again markedly better than its absolute accuracy; if all the runs were shown on a single Reynolds number *vs* Strouhal number plot, the discontinuity would probably not be apparent. This is, incidentally, probably why it has not been noticed by other workers.

As a result of a detailed consideration of the runs shown in figure 4 together with a number of similar runs, it is suggested that Roshko's formula be replaced by two sections of the form $SR = a + bR + cR^2$,

with a, b and c taking the following values:

	a	b	c
$50 < R < 105$	$-2{\cdot}1 \pm 0{\cdot}3$	$0{\cdot}144 \pm 0{\cdot}010$	$0{\cdot}00041 \pm 0{\cdot}00010$
$80 < R < 150$	$-6{\cdot}7 \pm 0{\cdot}2$	$0{\cdot}224 \pm 0{\cdot}006$	0 ($\lvert c \rvert < 0{\cdot}00025$)

The errors are a combination of standard errors of the mean and small estimated systematic ones. Those on a, b and c may be regarded as indicating how well the equation gives, respectively, the position, slope, and curvature of the varia-

tion. The uncertainty in a is thus the principal guide to how well the formulae determine the Strouhal number for a given Reynolds number. The errors on the two limbs are, of course, interdependent; the frequency difference between the two modes in the transition region may be given as

$$\Delta(SR) = 0{\cdot}7 \pm 0{\cdot}1.$$

The equation for the low-speed mode is likely to be biased in favour of the upper end of the range, since in many runs the speed at $R \sim 50$ was too low to be measured by tracing heat pulses.

At a speed in the range $80 < R < 105$, the frequency is likely to be found on one of the two lines rather than between them. The behaviour of the flow in this

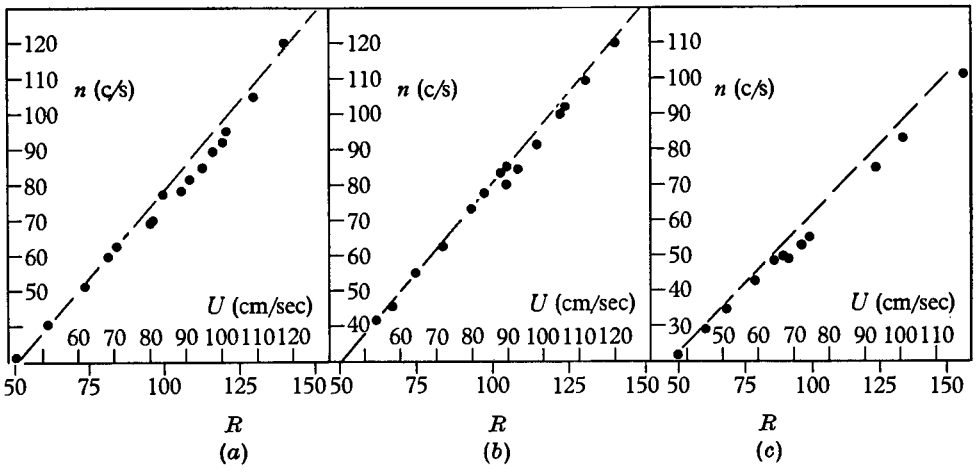

FIGURE 4. Three velocity-frequency plots showing the discontinuity. (*a*) Cylinder of diameter 0·178 cm, producing a long overlap between modes. (*b*) Same cylinder remounted, producing a sharp transition between modes, both frequencies being measurable at $U \sim 90$ cm/sec. (*c*) Cylinder of diameter 0·203 cm, with one point of intermediate frequency in transition region. The broken line in each plot is given by Roshko's formula.

transition region will be described more fully shortly, but, in connexion with the Reynolds number ranges for the two modes, it should be noted that when the low-speed mode occurred with $R > 95$, it almost always had irregularities. At lower speeds than this, irregularities could occur but did not necessarily do so.

All the above conclusions are based on wind-tunnel experiments. Water-channel investigations sometimes showed the transition beginning at speeds as low as $R = 70$.

Associated with the sudden decrease in frequency is a decrease in the intensity of the velocity fluctuations. (This probably means that the vortices are weaker, but could be due to the same amount of vorticity being more diffusely distributed.) This is shown in figure 5. At each speed a constant-current hot-wire anemometer 14·2 diameters downstream of the cylinder was traversed at right angles to the wake until the amplitude of its output was a maximum. This amplitude was then measured in arbitrary units (the scale on an oscilloscope screen) and plotted as

the ordinates of figure 5.* There is considerable scatter at the lowest speeds; apart from this, the graph shows an upward trend of amplitude with increasing speed on either side of a sharp drop. Simultaneous frequency measurements (figure 4*b*) showed that the flow changed from the low-speed mode to the high at the sharp drop; there was some unsteadiness in the frequency at 83·7 and 88·0 cm sec^{-1}, and at 90·1 cm sec^{-1} both frequencies were present, though it was possible to measure the amplitude of only the low-speed mode. That of the high-speed mode was clearly smaller.

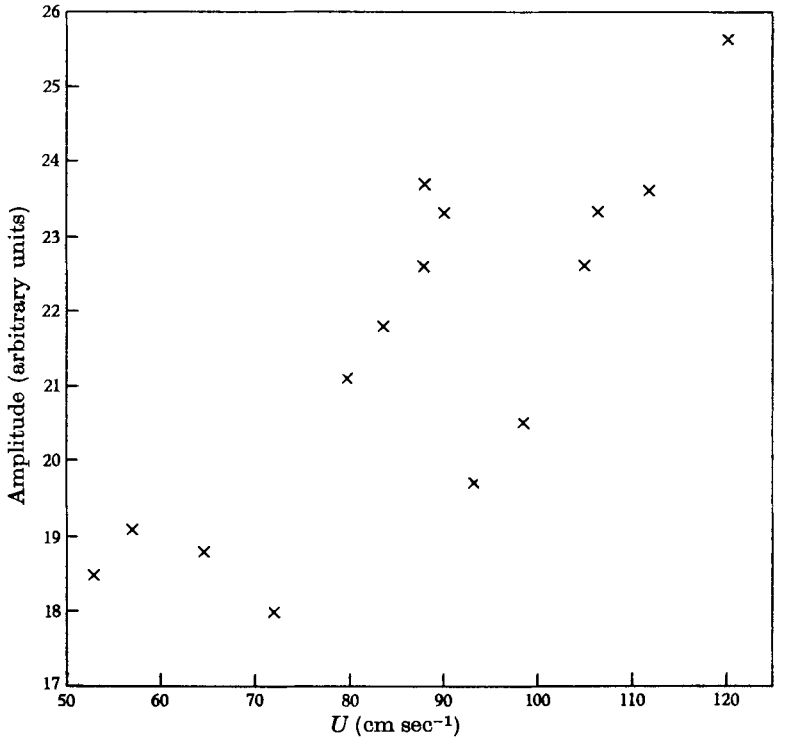

FIGURE 5. Plot of amplitude of output of constant-current hot-wire anemometer at amplitude maximum (with respect to y) against velocity for run shown in figure 4*b*.

The value of y (distance from the centre of the wake) was noted for each observation, but the maxima were too broad for any change in this at the transition to be detected.

2. Experimental arrangements

An investigation was carried out in the range of speeds between the two modes, where a more complex behaviour than either occurs. It shows a number of interesting features and, by indicating how each mode behaves when affected by the other, throws some light on the difference between the two. The observations

* Since the current through the hot-wire was held constant throughout the observations, the relationship between the velocity fluctuations and the observed amplitude depends in a complex way on the mean velocity (which is in any case an unknown quantity) at the position of the maximum. Only the discontinuity is significant in figure 5, not the form of the variation on either side of it. The constant-current method was chosen for experimental simplicity.

to be described suggest that the low-speed mode arises from an instability of the wake, whereas in the high-speed mode the vortex street is directly affected by the walls of the cylinder. The two modes have themselves been examined, as well as the transition between them, and some of the experiments show their contrasting features.

Experiments were carried out in both the wind-tunnel and a water-channel. The flow in the former was studied by making photo-traces of hot-wire outputs (with a drum-camera photographing an oscilloscope). The hot-wire probes used were of Wollaston wire with long unetched portions. This allowed the support to be outside the wake where it does not affect the street; it has been noted (see, for example, Kovasznay 1949) that distortion can be produced by having the support directly downstream of the wire, and I found that such an arrangement could even produce a change in the frequency when the wire was close to the cylinder. When only one wire was placed in the wake a time-scale could also be put on the photo-trace, but in a number of experiments both oscilloscope beams were used to indicate hot-wire outputs so that correlations between different positions in the wake could be studied.

The results could not be fully interpreted without visualization of the flow; the water-channel experiments, which I did not attempt to make quantitative, served this purpose. The channel used is open-topped, the water having a free surface. It enters through a 'honeycomb' which is followed by a short contraction before the working section. This does not give entirely uniform flow, but a cylinder of about 0·3 cm diameter placed vertically at the centre of the channel was clear of the velocity variations. The depth was about 14 cm, giving a length of about 30 diameters in which there were no wall or surface effects. The working section extended for about 20 cm beyond the cylinder before the flow was affected by the weir at the downstream end. Dye (potassium permanganate solution) was put into the flow through a small hole in the back of the cylinder producing the wake; this arrangement is better than putting the dye in upstream as it concentrates it close to the centre of rotation of each vortex and so gives a good picture of the motion of the vortices. (The dye comes away from the cylinder at the two separation points and thus gets into the regions of high vorticity.) This technique does not, of course, give any indication of three-dimensional effects. These were studied by using a cylinder coated with metallic tellurium; making this the cathode of an electrolytic cell (6 to 9 V between the cylinder and the walls of the channel proved satisfactory) produces marker all along the cylinder. The arrangement was similar to that in the dye experiments; because of the need to have the cylinder vertical, the vortex lines had to be viewed and photographed through a mirror.

In the water experiments, the approximate Reynolds number was determined from the eddy frequency.

3. Observations of the subcritical, critical and supercritical flows

Figure 6 (plate 1) shows the subcritical, critical, and supercritical flows (the term 'critical' being applied to the $R \sim 90$ transition). Photos 6*a* and *e* are of the low- and high-speed modes; both exhibit quite regular vortex streets. There is some

suggestion that in the high-speed mode the dye is less diffusely distributed, but this may be due to the fact that the same amount of dye was going into a faster flow. During the course of the experiment, I was unable to tell whether the flow was sub- or supercritical by looking at the vortices. A difference was apparent, however, when dye was put into the attached eddies (this was easily done by allowing the potassium permanganate to come out of the hole as a jet for a short while). Then in the low-speed mode the dye remained in the attached eddies (though there were oscillations of the vortex street frequency in this region), whilst in the high-speed mode it was removed by the fluctuations in a few cycles.

Photos 6*b*, *c* and *d* illustrate the critical flow. Irregularities of the type shown in 6*b* and *d* are a common feature of this flow. The pictures do *not* show a steady state. The irregularity first appears only a few diameters behind the cylinder (though only if dye is injected into the attached eddies can it be seen to affect these) and produces strongest lining-up (small or zero lateral separation of the vortices associated with increased longitudinal separation) at typically 20 diameters. The irregularity then travels further downstream with some reduction in the lining-up. The eddies upstream of this sometimes increase their lateral separation up to about 3/2 its normal value; this does not occur, however until typically 30 diameters behind the cylinder when the main part of the irregularity is still farther downstream. Photo 6*c* shows the same flow as 6*b* but between irregularities; one irregularity has just gone out of the picture downstream and another is just forming close to the cylinder.

Figure 7 (plate 2) shows the development of the irregularities as revealed by the wind-tunnel photo-traces. Even when the vortices have been largely dissipated by viscosity, the irregularities persist, thus producing some weak long time-scale turbulence.

Dye injected into the attached eddies in the transition flow stayed for some while and was then all removed very quickly. This could be regarded as the start of an irregularity. The dye removed in this manner went into the street a few eddies downstream of the ones that showed maximum lining-up.

The water-channel observations gave some indication that the irregularities travel upstream relative to the vortices. This is confirmed by wind-tunnel experiments with two hot-wires at different distances downstream (and separated slightly parallel to the cylinder so that one was not in the wake of the other); figure 8 (plate 2) shows a trace so produced. On average the irregularities had a velocity of about $0{\cdot}5U$ relative to the cylinder, though it varied considerably, occasionally going as low as $0{\cdot}3U$ and occasionally being very little less than U. There is some disagreement as to how fast the vortices themselves move—to take extreme examples, Tyler (1931) observed velocities mostly between $0{\cdot}7U$ and $0{\cdot}8U$, whilst Kovasznay's (1949) results imply a velocity of about $0{\cdot}98U$—but it is certainly faster than the irregularities.

Some two-wire experiments were also carried out with the separation in the y-direction. They showed, as the water-channel observations would lead one to expect, complete correlation of the irregularities across the wake.

It should be stressed that the behaviour being described here occurs not only

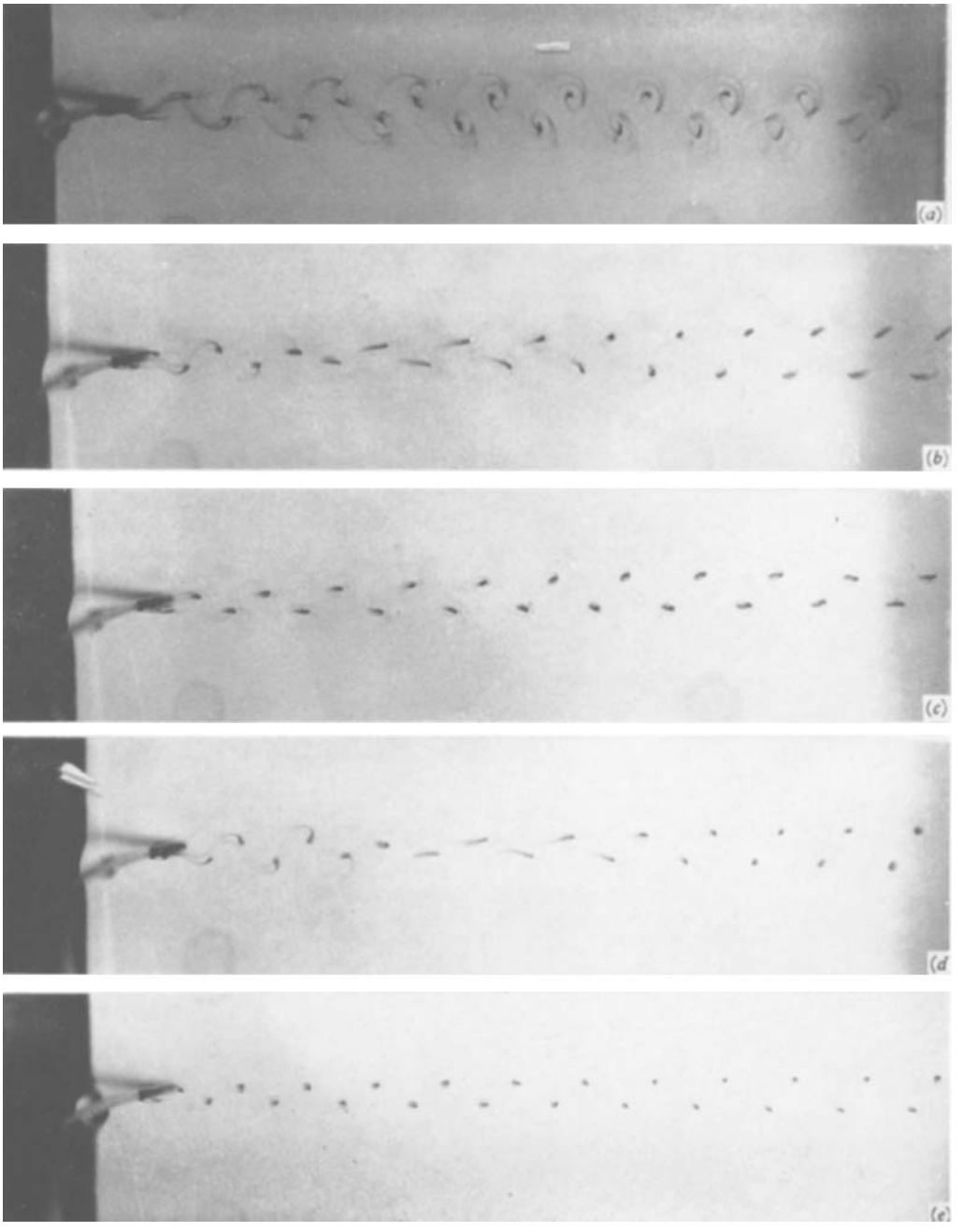

FIGURE 6. Water-channel photographs of the vortex streets (the cylinder is seen in perspective). (*a*) $R = 60$; low-speed mode. (*b*) $R = 75$; one of a sequence of randomly spaced irregularities. (*c*) $R = 75$; between irregularities. (*d*) $R = 79$; one of a periodic sequence of irregularities. (*e*) $R = 89$; high-speed mode.

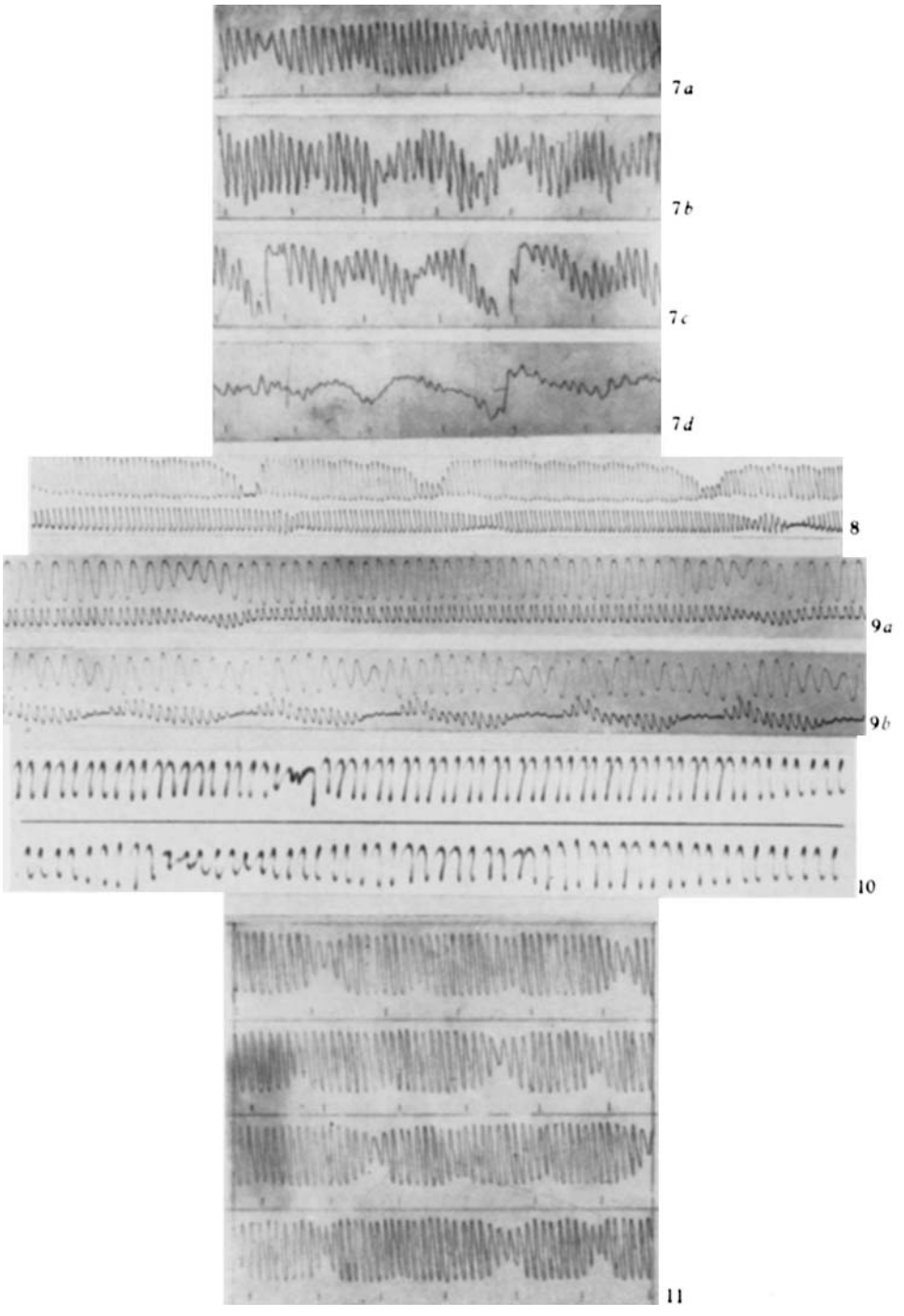

FIGURES 7 TO 11

DESCRIPTION OF PLATE 2

In all the photo-traces, time goes from left to right and, except where otherwise stated, the top corresponds to maximum velocity.

FIGURE 7. Photo-traces showing the development of randomly spaced irregularities as they travel downstream behind a cylinder of 0·178 cm diameter. The short lines on each trace mark 0·1 sec intervals. (*a*) $R = 102$; $x/d \sim 1{\cdot}5$; $y/d = 1{\cdot}0$. (*b*) $R = 101$; $x/d = 28{\cdot}5$; $y/d = 1{\cdot}8$. (*c*) $R = 104$; $x/d = 57$; $y/d \sim 2{\cdot}5$. (*d*) $R = 102$; $x/d = 104$; $y/d \sim 4$.

FIGURE 8. Simultaneous traces at different distances downstream behind a cylinder of diameter 0·178 cm, showing randomly spaced irregularities at $R = 105$. Upper trace—$x_1/d = 1{\cdot}5$; $y_1/d = 0{\cdot}7$. Lower trace—$x_2/d = 15{\cdot}7$; $y_2/d = 1{\cdot}0$ (the bottom corresponds to the maximum velocity). The separation of the irregularities on the two traces indicates the speed at which they travel downstream.

FIGURE 9. Photo-traces showing (*a*) randomly spaced irregularities and (*b*) periodically spaces ones, off-centre and at the centre of the wake. (*a*) $R = 98$; $x_1/d = x_2/d = 1{\cdot}5$; $y_1/d = 2{\cdot}5$; $y_2/d = 0$. (*b*) $R = 101$; $x_1/d = x_2/d = 14{\cdot}2$; $y_1/d = 2{\cdot}7$; $y_2/d = 0$. Note that in the two traces at the centre of the wake, the bottom corresponds to the maximum velocity.

FIGURE 10. Photo-trace showing intermittent jumps between the two modes. The two parts join straight onto one another. $R = 107$; $x/d = 15{\cdot}7$; $y/d = 1{\cdot}0$.

FIGURE 11. Photo-trace showing repetition of a complex pattern in the irregularities. The sequence of a large amplitude diminution followed after 10 wavelengths by a smaller one, then after another 11 wavelengths by an even smaller one, and then after 13 wavelengths by a large one, is repeated five times over. $R = 106$; $x/d \sim 1{\cdot}5$; $y/d = 1{\cdot}1$.

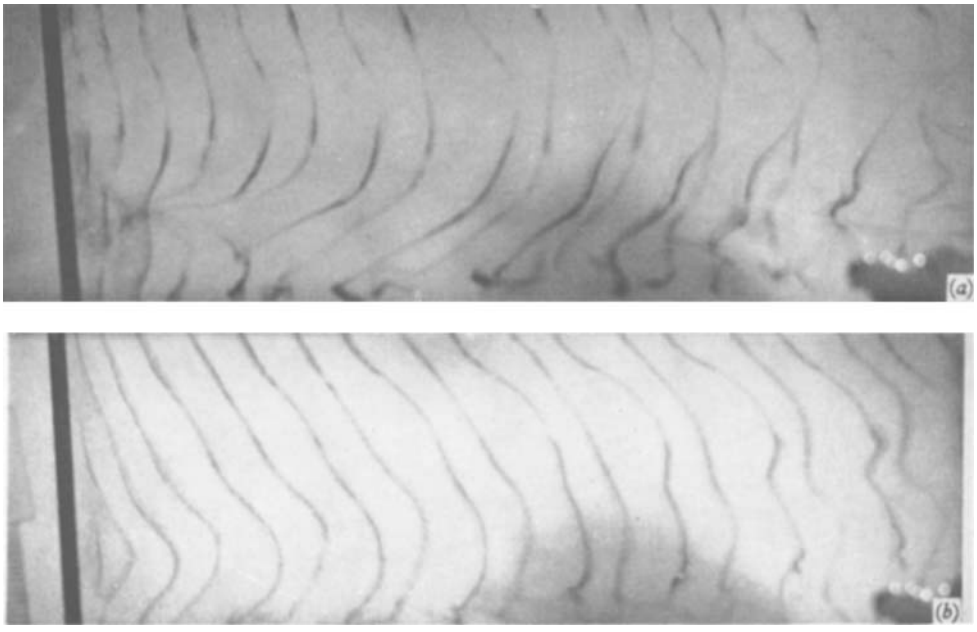

FIGURE 12. Tellurium experiments showing behaviour of the vortices parallel to the cylinder. (*a*) The occurrence of irregularities; $R = 78$. (*b*) High-speed mode, showing tendency for vortex lines to become wavy; $R = 88$.

when the flow changes from one mode to the other as a result of a speed change, but also as a repeated phenomenon when the Reynolds number is held in the short critical range between the two modes. A sequence of irregularities, usually similar to one another, with steady vortex streets between them, is then to be observed. The spacing can be either random or periodic. The flows shown in photos 6*b* and *d* differ in that in the former the irregularities were not evenly spaced, whereas in the latter they always had approximately 14 wavelengths between them. Figure 9 (plate 2) makes the same contrast for the wind-tunnel observations; photos 9*a* and *b* show the traces produced by a pair of hot-wires at the centre and a little off the centre of the wake for, respectively, random and periodic irregularities. Traces with a time-scale suggest that when the irregularities are randomly spaced the carrier frequency is that of the low-speed mode, and when they are periodic it is that of the high. In the latter case, considerable variation of the periodicity has been observed; the limits are about 6 and 14 wavelengths between consecutive irregularities. The frequency thus averages about twice the beat frequency of the two modes. I have not managed to relate the variations to any other feature of the flow.

The photo-traces revealed a wider variety of behaviour than the water-channel observations. Sometimes the amplitude modulation of a single carrier-frequency as described above did not occur at all; the transition region was then marked by a flow that would make sudden jumps from one mode to the other. These usually occurred too often for the frequencies between them to be measured on the photo-traces, but the modes could be identified by their different amplitudes (as in figure 10 (plate 2)); also the presence of the two frequencies could be detected by Lissajous figure observations on an oscilloscope. When this behaviour occurred the transition range was short, covering typically a difference of about 4 in Reynolds number (though there was considerable variation from one run to another of the position of this range).

More usually the transition flow occurred over a larger Reynolds number range of extent up to 10. The photo-traces then showed the more complex behaviour already discussed. Increasing the speed in small stages through the transition region could then produce in turn the low-speed mode modulated by random irregularities and the high-speed mode modulated by periodic ones. The former occasionally showed a striking repetition of a complex pattern in the irregularities, as illustrated by figure 11 (plate 2). This sort of odd behaviour is characteristic of the flow when it is in the low-speed mode at a speed at which it is normally in the high.

The photo-traces of figure 9 both show that at the centre of the wake the irregularities produce not only an amplitude modulation but also some variation in the mean velocity. This contrasts with the behaviour sufficiently far from the centre for the first harmonic to dominate; here the irregularities produce only amplitude modulation (together, of course, with the change in the spacing of the peaks corresponding to the increase in longitudinal spacing of the vortices). When the irregularities are periodic the mean velocity variation is almost sinusoidal. When they are random there is a peak shortly after each minimum in the amplitude (which is regarded as the main part of the irregularity); the

mean velocity does not change during the diminution. It thus appears that the irregularities have a flow into them from behind, a feature not apparent from the water-channel visualization. An alternative way of looking at this is to say that after the passage of an irregularity the flow is in a mode with a slightly different velocity profile at the centre of the wake from before and during its passage.

It is difficult to give a full interpretation of the photo-traces in terms of the observed motion of the vortex centres, as it is not clear how diffusely the vorticity is distributed; there is considerable difference between the velocity field of an ideal Karman street and one plotted out from experimental data (see, for example, Kovasznay (1949)). However, it seems satisfactory to associate the type of motion usually observed in the water-channel with the more complex of the transition features observed in the wind-tunnel. A different behaviour that also occurred in the water experiment, but only rarely, may then be associated with the sudden jumps between the modes. This different behaviour showed short transitions between the normal flow and a flow in which the eddies were very diffuse close to the cylinder, and in which some of the dye went into an amplified sinusoidal motion down the centre of the wake. This change did, of course, produce irregularities but they did not show the characteristics of the usual ones.

Presumably the exact behaviour in the transition region that occurs on any particular occasion is governed by small unobserved deviations from the theoretical arrangement. If the cylinder was slightly bent, a fairly complex motion always occurred. On the other hand, it was not always possible to produce a simple behaviour by taking care to make the cylinder straight.

The water-channel experiments on three-dimensional effects show that the irregularities are localized in the z-direction (parallel to the cylinder). This is shown in figure 12*a* (plate 3) in which one irregularity is just appearing close to the cylinder and another, at a different z, has travelled some distance downstream. An irregularity affects the flow for a distance of about six or eight diameters in the z-direction; outside this the vortex lines continue as normal.

The three-dimensional visualization was also examined to see whether it revealed any differences between the low- and high-speed modes. The differences are not so striking that they immediately revealed which mode the flow was in. There is, however, a general tendency for the vortex lines (identifying these with the observed lines of marker) to be straighter in the low-speed mode. This does not necessarily imply that the vortex lines are parallel to the cylinder in this mode; it requires only that the phase variation of the eddy production is proportional to z. In both modes angles of up to 30° or so between the vortex lines and the cylinder have been observed. However, vortex lines parallel or nearly parallel (at say $< 10°$) to the cylinder are more common in the low-speed mode than in the high. This tendency for the phase to be the same at different z for $R <$ about 90 but not for $R > 90$ has already been noted by Phillips (1956). In the high-speed mode any kinks in the vortex lines produced by the initial conditions are able to persist. Also, with increasing R there is a stronger tendency for bends to develop spontaneously (as illustrated by figure 12*b*); this is a trend towards the transition occurring at $R \sim 150$, when a three-

dimensional instability sets in producing both bends in the vortex lines and irregular motions of the vortices in the two-dimensional visualization.

The effect of a slight bend in the cylinder was investigated. The tendency for the bend to be reflected by a kink in the vortex lines is more marked in the high-speed mode than in the low.

The difference between the two modes was investigated with one further arrangement. The cylinder emitting dye through a small hole was used again, but with the hole at 90° to the front stagnation point. This was intended primarily to test the suggestion that the high-speed mode differs from the low in not possessing attached eddies; there would then be a single rear stagnation point of oscillating position. This is not the case, since the dye all left the cylinder wall at a single point some way in front of the rear generator in both modes; there were no oscillations of this point and no dye was carried across to the corresponding point on the other side. However, this arrangement did reveal a difference between the two modes further downstream. In the high-speed mode, the dye leaving the cylinder on one side of the wake went only into the vortices on that side. In the low-speed mode, on the other hand, there was a transfer of dye across the centre of the wake and it went almost equally into the two sides of the vortex street, though it was more diffusely distributed on the far side. It was thus clear that there was further development of the street downstream of the oscillating attached eddies, the street eddies being linked by an amplified sinusoid of dye. This feature was not shown by the high-speed mode.

With the hole between one of the separation points and the rear generator, most of the dye left the cylinder at the separation point on that side. A small amount was, however, transferred across to the other one, presumably by diffusion in the low-speed mode (dye can then accumulate in the attached eddies) and by the oscillations in the high-speed mode.

4. Effect of the transition on drag

The results of the experiments described in Part I have been examined to see whether the $R \sim 90$ transition affects the drag. As stated there, the U *vs* h curve for an individual fibre is more likely to reveal a change than the overall R *vs* C_D curve. The U *vs* h curve covering this Reynolds number is shown in figure 13. A glance along the points suggests that there might be a discontinuity in slope between $U = 1000$ and $1100\ \mathrm{cm\ sec^{-1}}$, which correspond respectively to $R = 76{\cdot}5$ and $84{\cdot}0$. Since, however, the evidence for the discontinuity is not wholly convincing, the points have been analysed statistically, by making least squares fits of the points on either side of the suspected discontinuity to quadratics,* and comparing the differences in the coefficients with their standard errors. No significant discontinuity in slope was indicated, but the results did indicate a discontinuity, significant at the 5 % level, in the actual value of h. The change was upwards with increasing U. This suggests that the transition does have some effect on the drag, but it is not evident just what. The point at $U = 1016$

* The origin, which is, of course, necessarily a point, was *not* included, as it would clearly have strongly influenced the fit and the logarithmic nature of the low Reynolds number solutions indicates that it would not fit in with any quadratic approximation.

cm sec^{-1}, which has a particularly high h, is obviously strongly influencing the result, and it may be that this point is in the transition region and should not be included in either fit (the analysis indicating the discontinuity includes it in the high velocity one). Clearly, further experiments are required, and the author hopes to be able to do these in due course.

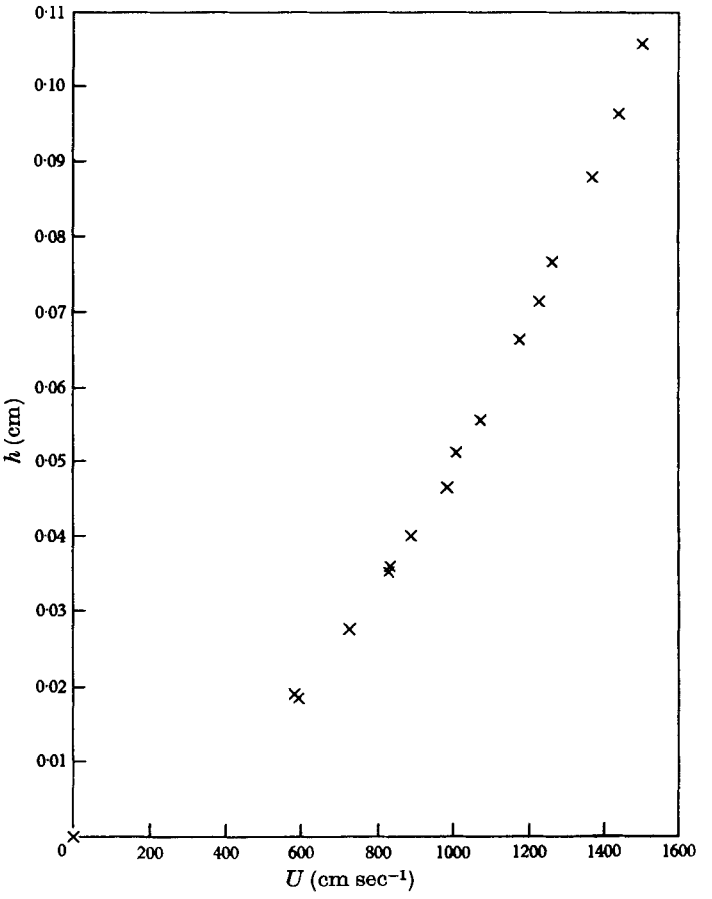

FIGURE 13. Velocity-deflexion curve for fibre 8.

5. Discussion

The most satisfactory explanation of the $R \sim 90$ transition seems to be the following. The first appearance of the vortex street at $R \sim 40$ is the result of an instability of the wake; the only role of the cylinder is to produce the velocity profile. The reason that the instability gives rise to a persisting periodic motion rather than turbulence is probably that the Reynolds number (based on the wake itself—not the cylinder producing it) is independent of the distance downstream; this contrasts with a two-dimensional jet in which the Reynolds number increases with x. For the same reason, it is to be expected that the beginning of instability will be close to the cylinder.

As the speed is increased, the development from this first appearance to a full vortex street is compressed more and more into a region just behind the cylinder

until the formation of the street is directly affected by its walls. The attached eddies might also have an effect, but since the velocity profiles in this region are similar to those further downstream except for their crossing the zero line (Kovasznay 1949; Kawaguti 1953) this is unlikely.

In the transition region the effect of the walls is only partial, but, when the flow is in the high-speed mode the origin of the vortex street is in the immediate vicinity of the cylinder. It no longer grows from an instability of a given velocity profile, so that the factors governing its parameters (frequency, spacing of eddies, etc.) are different. Frequency and amplitude discontinuities at the transition are thus plausible.

On either side of the critical Reynolds number, there are oscillations with the vortex street frequency of the attached eddies. The distinction is that, in the low-speed mode, these oscillations are produced by the beginnings of an instability which develops further as it goes downstream, whereas, in the high, a fully developed vortex street exists right from its start close to the cylinder. In the low-speed mode the same fluid remains in the attached eddies throughout, whilst in the high the fluid there is continually moving into the vortex street; only then is the common way of speaking of the vortex street being produced by shedding of the attached eddies strictly correct.

These conclusions imply that attempts to provide a theoretical derivation of the parameters of the vortex street must be differently based for the two modes. The well-known treatment by von Kármán (see Lamb 1932, § 156) of an infinite double row of equal point vortices provides primarily an explanation of why the street, once formed, should be stable; the reasons for the formation with a spacing-ratio fairly close to the theoretical stability requirement must lie in the mechanism of the formation. For the low-speed mode a stability theory of the wake seems likely to be appropriate. Hollingdale (1940) has developed such a theory for a parallel wake with $R \to \infty$ and attempted a comparison with experiments on wakes of flat plates at zero incidence and aerofoils. The comparison is difficult because of changes in the wake with distance downstream and this difficulty is likely to be even more marked for the cylinder. However, the partial success of Hollingdale's comparison, together with Taneda's (1958) observation that the wakes of plates and cylinders behave similarly, once they are clear of the direct influence of the walls, does suggest that an instability of the wake could give the observed value of the longitudinal spacing. For the high-speed mode, on the other hand, the above interpretation suggests that the eddy frequency is governed by the oscillations in the immediate vicinity of the cylinder; this, together with the speed with which the eddies travel downstream, then determines the longitudinal spacing. Birkhoff's (1953) rough derivation of the Strouhal number by considering the wake swinging from side to side as a solid simple harmonic oscillator might apply here, though it should be remembered that the attached eddies now consist of continually changing fluid.

There is one quantity that can be crudely estimated for either of these ideas about the origin of the street, namely the lateral spacing. Eddies produced by a wake instability are likely to have their centres close to the points of inflexion in the velocity profile (more specifically, the laminar profile at the origin of the

instability); the experimental profiles given by Kovasznay (1949) indicate that these are between 0·9 and 1·5 diameters from the centre line. On the other hand, eddies produced close to the cylinder are likely to be at about the same y as the maximum vorticity there; Kawaguti's (1953) numerical solution suggests that this is in the range 0·4–0·8 diameters. Observed lateral separations in the two modes (as in photos 6*a*, *e*, and other similar ones) are consistent with these interpretations; so too are wind-tunnel observations of the position of maximum amplitude (though it is not clear just how this position is related to the centre of rotation). In each mode, however, there is a continuous decrease of lateral separation with increasing Reynolds number, so that the observations may not be specifically a feature of the two modes; there was too much scatter for any discontinuity in the lateral separation at the transition to be detected.

Although there is no direct evidence on this point, the data seem to require a discontinuity in the longitudinal separation. For a von Kármán ideal vortex street the frequency is related to the longitudinal and lateral spacings s_1 and s_2, the strength of each vortex κ, and the free stream velocity U by

$$n = \frac{U}{s_1} - \frac{\kappa}{2s_1^2} \tanh \frac{\pi s_2}{s_1}.$$

It is known that n decreases at the transition, and the indications are that κ and s_2 both decrease. Since the second term is always small compared with the first, s_1 must increase. This contrasts with its general trend, which, like that of s_2, is downwards with increasing Reynolds number.

This change in longitudinal spacing is thought to be the root of the behaviour of the transition flow. If the speed is such that the high-speed mode is just beginning to produce vortices but their motion downstream is governed by the wake instability, then they will take up a longitudinal spacing that is too small for the rate at which they are being produced. This can continue only for a short while; there will then be a compensating region of increased longitudinal spacing, which could well produce the sort of irregularity shown in figures 6*b* and *d*. In all the photographs, such as these two, the vortices in an irregularity line up with those downstream of it more smoothly than with those upstream. This suggests that the street is forced into the large spacing of an irregularity by the rate at which vortices are formed, and then breaks off and starts anew in the mode with the small spacing.

Since, when the irregularities are randomly spaced, the carrier frequency is the low-speed mode, the flow is then presumably only intermittently inclined to produce vortices at the supercritical frequency. At slightly higher speeds they are continuously produced at this frequency, but still pulled into the subcritical spacing; the irregularities are then periodic. It is plausible that, in these circumstances, each one should take about the same time to develop, but attempts to produce a full theory of the periodicity have been unsuccessful.

The above remarks have, for the sake of simplicity, treated the behaviour as two-dimensional. It should be remembered that, in fact, the irregularities are localized in the third dimension. The return to regular street after an irregularity is probably brought about by the undistorted vortex lines on either side.

An alternative interpretation of the transition as the first onset of three-dimensional instability has been rejected, because it seems unlikely that this would produce supercritical streets as regular as the subcritical ones (compare photos 6*a* and *e*). The three-dimensional differences between the two modes, described earlier, are thought to be due to the high-speed mode being more directly affected by conditions at the cylinder than the low. The behaviour at $R \sim 150$ suggests that the beginning of three-dimensional instability occurs there.

My gratitude is expressed to all the members of the fluid mechanics group in the Cavendish Laboratory who have contributed in discussions to my understanding of the problem; I must mention by name Dr A. A. Townsend. I am also grateful to Mr A. M. Walker of the Cambridge University Statistical Laboratory who suggested the significance tests in § 4 of Part II and carried out the computations involved, and to Mr W. E. Thompson for his help in making apparatus. The water-channel used is in the hydraulics department of the Cambridge University Engineering Laboratories and my thanks go to all there for their co-operation. I also wish to acknowledge receipt of a maintenance grant from the Department of Scientific and Industrial Research.

REFERENCES

ALLEN, D. N. DE G. & SOUTHWELL, R. V. 1955 *Quart. J. Mech. Appl. Math.* **8**, 129.
APELT, C. J. 1959 *Rep. and Memo., Aero. Res. Counc., Lond.* (To be published.)
BAIRSTOW, L., CAVE, B. M. & LANG, E. D. 1923 *Phil. Trans.* A, **223**, 383.
BIRKHOFF, G. 1953 *J. Appl. Phys.* **24**, 98.
GOLDSTEIN, S. (ed.) 1938 *Modern Developments in Fluid Dynamics.* Oxford University Press.
HOLLINGDALE, S. H. 1940 *Phil. Mag.* (7), **29**, 209.
HOMANN, F. 1936 *Forsch. Geb. IngWes.* **7**, 1.
KAPLUN, S. 1957 *J. Math. Mech.* **6**, 595.
KAWAGUTI, M. 1953 *J. Phys. Soc. Japan*, **8**, 747.
KOVASZNAY, L. S. G. 1949 *Proc. Roy. Soc.* A, **198**, 174.
LAMB, H. 1911 *Phil. Mag.* (6), **21**, 112.
LAMB, H. 1932 *Hydrodynamics*, 6th edn. Cambridge University Press.
NISI, H. & PORTER, A. W. 1923 *Phil. Mag.* (6), **46**, 754.
PHILLIPS, O. M. 1956 *J. Fluid Mech.* **1**, 607.
PRANDTL, L. (ed.) 1923 *Ergebn. Aerodyn. VersAnst. Göttingen*, **2**, 23.
PROUDMAN, I. & PEARSON, J. R. A. 1957 *J. Fluid Mech.* **2**, 237.
RELF, E. F. 1913 *Tech. Rep. and Memo., Adv. Comm. Aero.* (*A.R.C.*), *Lond.*, no. 102.
ROSHKO, A. 1954 *Rep. Nat. Adv. Comm. Aero., Wash.*, no. 1191.
SCHMIDT, E. 1934 *Proc. 4th Int. Congr. App. Mech.* (*Camb.*), p. 92.
SCHMIDT, E. & BECKMANN, W. 1930 *Tech. Mech. Thermodynam.* **1**, 341, 391.
SOUTHWELL, R. V. & SQUIRE, H. B. 1934 *Phil. Trans.* A, **232**, 27.
TANEDA, S. 1956 *J. Phys. Soc. Japan*, **11**, 302.
TANEDA, S. 1958 *J. Phys. Soc. Japan*, **13**, 418.
THOM, A. 1929 *Rep. and Memo., Aero. Res. Coun., Lond.*, no. 1194.
THOM, A. 1933 *Proc. Roy. Soc.* A, **141**, 651.
TOMOTIKA, S. & AOI, T. 1950 *Quart. J. Mech. Appl. Math.* **3**, 140.
TRITTON, D. J. 1959 *Phil. Mag.* (in the Press).
TYLER, E. 1931 *Phil. Mag.* (7), **11**, 849.
WIESELSBERGER, C. 1921 *Phys. Z.* **22**, 321.
WIESELSBERGER, C. 1922 *Phys. Z.* **23**, 219.